Water Research 176 (2020) 115743

Contents lists available at ScienceDirect

Water Research

journal homepage: www.elsevier.com/locate/watres

Characterization of organic matter by HRMS in surface waters: Effects of chlorination on molecular fingerprints and correlation with DBP formation potential

Josep Sanchís [a, b, *], Adrián Jaén-Gil [a, b], Pablo Gago-Ferrero [a, b], Elias Munthali [a, b], Maria José Farré [a, b, **]

[a] Catalan Institute for Water Research (ICRA), Scientific and Technological Park of the University of Girona, H2O Building, C/Emili Grahit, 101, E17003, Girona, Spain
[b] University of Girona, 17071, Girona, Spain

ARTICLE INFO

Article history:
Received 8 January 2020
Received in revised form
16 March 2020
Accepted 20 March 2020
Available online 25 March 2020

Keywords:
High resolution mass spectrometry
Water chlorination
Dissolved organic matter
Disinfection by-products
van krevelen diagram
DBP formation Potential

ABSTRACT

In order to understand and minimize the formation of halogenated disinfection by-products (DBPs), it is important to investigate how dissolved organic matter (DOM) contributes to their generation. In the present study, we analysed the DOM profile of water samples from the Barcelona catchment area by high resolution mass spectrometry (HRMS) and we studied the changes after chlorination. Chlorination produced significant changes in the DOM, decreased the average m/z and Kendrick mass defect (KMD) of their spectra and decreased the number and abundance of lignin-like features. The Van Krevelen (VK) fingerprint exhibited several noticeable changes, including the appearance of highly oxidized peaks in the tannin-like region (average O/C, 0.78 ± 0.08), the appearance of features with low H/C and the disappearance of more than half of the lipids-like features. Up to 657 halogenated peaks were generated during sample chlorination, most of which in the condensed hydrocarbons-like and the lignin-like region of the VK diagram.

Around 200 features were found to be strongly correlated ($\rho \geq 0.795$) to the formation potential of trihalomethanes (THMs) and 5 were correlated with the formation potential of haloacetonitrile (HANs). They all were plotted in the lignin fraction of the VK diagram, but both groups of features exhibited different nitrogen content: those features related to HANs FP had at least one nitrogen atoms in their structures, whilst those related to THMs did not.

1. Introduction

Water chlorination is an efficient and cost-effective method for removing pathogens related to waterborne diseases, such as typhoid fevers, cholera, botulism and dysentery. Its introduction in the early 20th century (EPA.US, 2000; Leal et al., 1909; Traube, 1894) is regarded as a major turning point in the history of water management. Notwithstanding the sanitary benefits of water chlorination, the addition of disinfectants to water triggers the generation of a myriad of disinfection by-products (DBPs), some of which are carcinogenic and may cause several toxicological effects after chronic consumption, even at trace levels (Font-Ribera et al., 2018; Villanueva et al., 2015). Subsequently, the occurrence of halogenated DBPs derived from water chlorination is an emerging concern and several regulations have been enacted, at domestic and supranational level, to minimize the exposure of population to them (Chinese Department of Health, 2006; Commission, 1998; European Parliament, 2000; NHMRC and NRMMC, 2011; US-EPA, 2006, 1998).

Brominated and chlorinated trihalomethanes (tribromo-, trichloro-, bromodichloro- and dibromochloromethane), also known as THMs, have attracted the most attention of both, academia and regulatory agencies, but the list of identified halogenated DBPs contains hundreds of molecules from families as diverse as

* Corresponding author. Catalan Institute for Water Research (ICRA), Scientific and Technological Park of the University of Girona, H2O Building, C/Emili Grahit, 101, E17003, Girona, Spain.
** Corresponding author. Catalan Institute for Water Research (ICRA), Scientific and Technological Park of the University of Girona, H2O Building, C/Emili Grahit, 101, E17003, Girona, Spain.
E-mail addresses: jsanchis@icra.cat (J. Sanchís), mjfarre@icra.cat (M.J. Farré).

https://doi.org/10.1016/j.watres.2020.115743

haloacetic acids, haloacetonitriles, haloketones, haloaldehydes, halonitromethanes, and haloacetamides, among others (Richardson et al., 2008). Recently, the use of non-target analyses has revealed the existence of a high number of previously unknown halogenated DBPs in drinking water (Richardson and Ternes, 2018). High resolution mass spectrometry (HRMS) and ultrahigh resolution mass spectrometry (UHRMS) analyses have contributed to determine their elemental composition through highly accurate *m/z* measurements (Zhang et al., 2014, 2012; Zhang and Yang, 2018).

Adsorbable Organic Halides (AOX) analyses often report the presence of a significant number of halogenated substances, the structures of which are yet to be elucidated. Hua and Reckhow observed that only ~45% of the total AOX could be explained by the presence of THMs, trihaloacetic acids and dihaloacetic acids (Hua and Reckhow, 2007); while Yeh et al. observed that the percentage of AOX that could be justified by the occurrence of targeted DBPs was rather variable (35–118%) in swimming pool water (Yeh et al., 2014). Finally, an unsettled amount of DBPs, halogenated or not, may be generated during water chlorination without being detectable by AOX or by conventional extraction and detection methods.

Direct measurements of target DBP are undoubtedly useful. However, the prediction of the DBP formation potential (FP) is equally important, particularly in those cases when adjusting the disinfection parameters is viable. In this regard, the characterization of dissolved organic matter (DOM) has proved to be a promising tool. Several DOM properties are closely related to the occurrence of DBP precursors (such as THMs), and/or can be used as descriptors for predicting their FPs. This includes DOM's spectroscopic properties (i.e., ultraviolet absorbance at $\lambda = 254$ nm or $SUVA_{254}$ (Hua et al., 2015) and fluorescent signal (Roccaro et al., 2009)), its composition (e.g., the presence of protein-like organic matter (Chu et al., 2010), aromatic moieties (Hua et al., 2015), and suspended particulate matter (Hou et al., 2018)), and the bulk concentration of DOM, which can be accounted as total organic carbon, TOC (Lee et al., 2009), or as dissolved organic carbon, DOC (Peng et al., 2016).

Commonly, predictive models are multi-parametrical and contemplate a wide range of physicochemical conditions (i.e. the concentrations of halide ions or the pH), as well as chlorination parameters (the reaction time, the temperature, the reagent dose, etc.) (Sohn et al., 2004). However, these models mostly rely on a reduced number of selected DBP. Target methods can hardly cover the quantitative analysis of the whole set of DBPs generated during water chlorination, because of (i) the large number of identified DBPs, (ii) the elevated costs of obtaining high purity standards for all of them, and (iii) the presence of unknown DBPs. Therefore, the risk of DBPs formation should be addressed using more holistic approaches, such as non-target analyses based on HRMS. The advances in mass spectrometry (MS) have allowed the identification of individual components of DOM, which is one of the most heterogeneous mixtures in the environment (Woods et al., 2009). High-field-strength Fourier Transform Ion Cyclotron Resonance MS (FTICR-MS) is capable of unravelling complex DOM mixtures across aquatic systems (Kellerman et al., 2014; Riedel et al., 2016), and Orbitrap-MS has proven to be a valid alternative, as it also is capable of detecting subtle changes in DOM profiles, despite of being able to assign fewer features due to its lower m/z resolution power (Farré et al., 2019; Hawkes et al., 2018, 2016; Patriarca et al., 2018; Yuthawong et al., 2019). The HRMS study of DOM is often complemented with graphical representations ("fingerprinting"), such as van Krevelen (VK) diagrams and Kendrick Mass Defect (KMD) plots, which assist in the visualization, interpretation and comparison of DOM profiles (Andersson et al., 2019; Kim et al., 2003; Lavonen et al., 2013).

The objective of the present study was to investigate the changes of the DOM after water chlorination from a multivariate analysis perspective and exploring the changes in their fingerprint, obtained with Orbitrap-MS, in order to (i) understand which regions of the fingerprints were more susceptible to changes during disinfection reactions and (ii) to identify surrogate features to help predicting DBP formation. To this aim, we extracted and analysed the DOM of ten surface water samples from Barcelona catchment area. DOM was isolated by solid-phase extraction (SPE) and analysed by HRMS. Instrumental analyses were conducted before and after lab scale chlorination tests, in order to track the changes in the DOM. The method was finally validated by investigating the correlation between *m/z* features and the concentrations of two families of halogenated DBPs: THMs and haloacetonitriles (HANs), chosen because of their relevance, hazardousness and representativeness in real drinking waters.

2. Methods and materials

2.1. Standards and reagents

HANs standards were obtained as a mix at 5.0 mg/mL in acetone (>95% purity) from Cluzeau (Sainte-Foy-la-Grande, France). THMs were purchased as a 1.0 mg/mL mix in methanol (TraceCERT® grade) from Sigma Aldrich. Deuterated 1,2-dibromopropane-d_6 (99.6 atom % D) was purchased from CDN isotopes (Quebec, Canada) and used as internal standard during DBP analyses (see details in the supporting information, Text S1).

Ultrapure water and methanol (Optima® LC/MS grade) were purchased from Fisher Chemical (Geel, BE, and Loughborough, UK, respectively). Methyl *tert*-butyl ether (MTBE, Chromasolv™ Plus), NaClO (6–14% active chlorine, Emplura® grade) and formic acid 98–100% (ACS/Reag. Ph Eur grades) were acquired from Merck (Darmstadt, Germany). Sulphuric acid 95–97% (Reag. Ph Eur grade) was obtained from Scharlau (Sentmenat, Spain).

Na_2SO_4 (≥99.0%, ACS grade) and anhydrous Na_2SO_3 (≥98.0%, BioUltra grade) were obtained from Sigma-Aldrich (ref. 239313). NaOH pellets (PA/ACS/ISO grades) were acquired from Panreac (Barcelona, Spain). KH_2PO_4 (ACS/ISO/Reag. Ph Eur grades) was obtained from Scharlau (Sentmenat, Spain). Nitrogen (99.995% purity) for extract drying was purchased from Abelló Linde (Barcelona, Spain).

Glass fibre filters (GF/F, 47 mm diameter, 0.7 μm mesh size) were obtained from Whatman (Little Chalfont, UK). Bond Elut PPL ("*Priority PolLutant*") cartridges (500 mg, 3 mL; reference 12105006) were purchased from Agilent Technologies (Santa Clara, CA, USA).

2.2. Sampling

The sampling was carried out in the Ter River Basin (NE of Spain, see Fig. 1) in February 2019. Samples were taken from the Ter River itself and from the three reservoirs Sau, Susqueda and Pasteral (169 hm^3, 233 hm^3 and 2 hm^3, respectively). These reservoirs are relevant for the Barcelona metropolitan area, as they supply around 170 hm^3 drinking water (Agència Catalana de l'Aigua, 2015)) through interbasin water transfer, and present certain differences in term of morphology, trophic state and residence time (with Sau being the most eutrophic water body of the reservoirs chain), all of which may have a potential impact in the nature and concentration of DBP precursors.

Samples were taken at the specified depth (see Table 1) in amber glass bottles letting no head-space. The bottles were immediately refrigerated and transported to the laboratory, where they were processed within 24 h following the general procedure

Fig. 1. Maps Location of the sampled waterbodies in Catalonia (*a*). The Ter River basin is highlighted in red (*b* and *c*), while the Sau, Susqueda and Pasteral reservoirs are highlighted in blue, black and green, respectively (*c*). Geodata obtained from Catalan Water Agencies website (Agència Catalana de l'Aigua, 2019). (For interpretation of the references to colour in this figure legend, the reader is referred to the Web version of this article.)

schematized in Fig. 2 and described in the following sections.

2.3. Batch chlorination experiments

The DBP FP was assessed following a modified version of the standard method (APHA, 2005) to obtain between 1 and 3 mg/L of residual free chlorine after 24 h of contact time as described in previous studies (De Vera et al., 2015; Doederer et al., 2014; Liu et al., 2016). Once determined, the specific chlorine dose was added to a 250 mL head-space free glass bottle. The bottle was capped and stored in an incubator, in the dark, at 25 °C, for 24 h. The residual chlorine was measured with a photometric cuvette test kit (LCK 310, Hach Lange GmbH, Düsseldorf, Germany). After measuring their chlorine content and quenching them with ascorbic acid, samples were extracted for DBP analysis (see Text S1 in the Supporting information) and for DOM characterization (see section 2.4).

2.4. Extraction of PPL-DOM

Raw and quenched chlorinated samples were processed following the same protocol. Aliquots of each sample were filtered through 0.7 μm mesh-size glass fibre filters and extracted by SPE according to the method described elsewhere (Dittmar and Koch, 2006) with minor modifications, as previously implemented in Farré et al. (2019). Briefly, 250 mL of filtered sample were acidified to pH 2.0 by adding formic acid drop by drop and were extracted with a PPL cartridge (500 mg, 3 mL). These cartridges contain a styrene-divinylbenzene polymeric phase, modified with a non-polar surface. Recent studies have shown that PPL-cartridges are found among the most efficient sorbents for DOM components, enabling a broad coverage of DOM constituents in one single collection while avoiding substantial leaching (Li et al., 2017), and

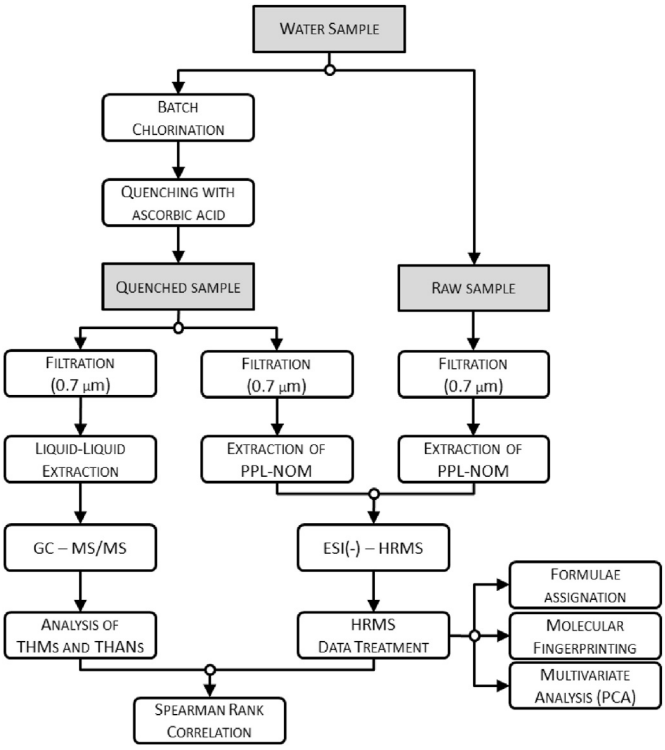

Fig. 2. Scheme of the experimental design.

Table 1
Summary of analysed samples.

Code	Water Body	Depth (m)	TOC (mg/L)	TN (mg_N/L)	THMs FP (μg/L)	HANs FP (μg/L)
TER	Ter River	0	2.0	5.7	33.6	1.4
PAS	Pasteral Reservoir	0	3.7	2.7	55.8	3.1
SAU_0m	Sau Reservoir	0	2.7	4.2	38.5	2.9
SAU_13m	Sau Reservoir	13	2.9	4.2	48.1	3.1
SAU_30m	Sau Reservoir	30	2.7	4.8	56.9	5.1
SAU_42m	Sau Reservoir	42	2.7	5.0	44.7	4.5
SUS_0m	Susqueda Reservoir	0	3.3	2.7	57.8	3.6
SUS_8m	Susqueda Reservoir	8	3.3	2.7	57.5	3.9
SUS_35m	Susqueda Reservoir	35	3.4	2.7	73.6	4.8
SUS_80m	Susqueda Reservoir	80	3.4	2.7	75.9	5.1

they have been extensively applied to extract and characterize DOM from several water matrices (Arakawa et al., 2017; Farré et al., 2019; Li et al., 2016).

Prior to the extraction, cartridges were washed thrice with 1.0 mL of methanol and were soaked overnight with 1.0 mL of methanol. After being conditioned, the cartridges were washed with one volume of formic acid 0.1% v/v. Then, samples were loaded, under vacuum at approx. 2 mL/min. Salts were rinsed off with 3.0 mL of formic acid 0.1% v/v and cartridges were dried under vacuum for 15 min. Finally, the elution was carried out with 2.00 mL of methanol. The extracts were collected in previously tared liquid chromatography (LC) vials. 500 μL of the methanolic extracts were diluted 1:1 with ultrapure water and stored at −20 °C until their instrumental analysis.

Procedural blanks consisting of 250 ± 1 mL of ultrapure water were filtered and extracted following the same protocol and in parallel with real samples analyses. Quenched chlorination blanks were also processed.

2.5. Instrumental analysis of organic matter

Analyses were carried out by HRMS using a LTQ Velos™ from Thermo Scientific (San José, CA, USA), using a hybrid Linear Ion Trap − Orbitrap analyser.

Extracts of blanks, raw samples and chlorinated samples were infused into the mass spectrometer at a flow of 8 μL/min. The ionisation was performed with an electrospray ionisation (ESI) source operating in negative polarity. The instrumental parameters were set as follows: the capillary voltage was set at −3.1 kV; the capillary and the source heater temperatures were maintained at 275 °C and 45 °C, respectively; the sheath gas and the auxiliary gas flows were set at 28 and 5 a.u., while the sweep gas flow was turned off. 300 scans were acquired for every sample. Spectra were acquired in full-scan mode, with a resolution of 100,000 Da FWHM and a *m/z* range of 100–1000. The following signals were used as lock masses for internal calibration during spectra acquisition: *m/z* 369.08272 ($[C_{16}H_{17}O_{10}]^-$), *m/z* 397.11402 ($[C_{18}H_{21}O_{10}]^-$) and *m/z* 423.12967 ($[C_{20}H_{23}O_{10}]^-$).

2.6. Data treatment: determination of elemental compositions and fingerprinting

An averaged spectrum of each sample was obtained using the software Xcalibur™ 2.2 (Thermo Scientific). Spectra were exported as Excel Workbook format files and processed with a custom script in R (v. 3.5) using the RStudio environment (v. 1.1.463, R-Tools Technology).

The elemental compositions of the spectral signals were tentatively determined with functions from the R package MFAssignR (Schum et al., 2019). The workflow is fully described in the Supporting information (Text S2). Briefly, *m/z* signals were assigned to elemental formulae ($CHON_{0-5}S_{0-2}Cl_{0-2}Br_{0-2}$) using the function MFAssignR:MFAssign with the following restrictions: maximum tolerable *m/z* error: ±1.0 ppm; *m/z* range: 100–1000; charge: only monocharged formulae were considered; range of O/C: 0–1.0; range of H/C: 0.3–2.5; range of DBEO: 1–10.

The presence of features with ^{32}S, ^{35}Cl or ^{79}Br atoms was double-checked by searching isotopologues containing ^{34}S, ^{37}Cl and ^{81}Br, respectively. The experimental $^{37}Cl/^{35}Cl$, $^{34}S/^{32}S$ and $^{81}Br/^{79}Br$ ratios were compared to natural isotopic ratios as detailed in Text S2.

The final list of formulae was represented in VK diagrams based on their O/C, H/C and N/C ratios. They were classified in predefined categories according to their location in the VK diagram. These classification criteria, detailed in Table S1, have been accepted in a multitude of recent DOM studies, although it should be noted that they may not fully describe the structural diversity of the peaks that are contained in each compositional space, and it should be stressed that further structural elucidation should be performed to identify each substance and to unambiguously classify it (Schymanski et al., 2014).

The aromaticity index (AI) of each formula was calculated according to equation (1) (Koch and Dittmar, 2006):

$$AI = (1 + C - O - S - 0.5 \times H) \,/\, (C - O - S - N - P) \quad (1)$$

The double bound equivalent (DBE), normalized by the number of carbons, was calculated according to equation (2) (Melendez-Perez et al., 2016):

$$DBE \,/\, C \;= [1 + 0.5 \times (2 \times C - H + N)] \,/\, C \quad (2)$$

Masses were transformed to Kendrick mass (KM) values by normalizing their IUPAC (^{12}C based) mass by 1.0011178 ($KM_{CH2} = 1.0000000$) (Kendrick, 1963). Then, KMD were calculated as in equation (3) (Hughey et al., 2001) and KMD plots were presented:

$$KMD \;= KM - \lfloor KM \rfloor, \quad (3)$$

where KM and $\lfloor KM \rfloor$ stand for the Kendrick mass (KM) and the truncated Kendrick mass values, respectively.

2.7. Data treatment: descriptive statistics and multivariate analyses

Statistics and multivariate analyses were performed using the R packages *vegan* (Oksanen et al., 2019), *stats* (R Core Team, 2019) and *FactoMineR* (Lê et al., 2008), among others.

The data normality was checked using Shapiro–Wilk tests and the null hypothesis (H_0) was rejected when $p \leq 0.05$. Differences among raw samples and chlorinated samples were investigated using paired difference tests: Non-normally distributed data was assessed with Wilcoxon signed-ranks tests, while paired Student's *t*-tests were applied to normal datasets. In both cases, differences were considered significant at p values ≤ 0.05. In multiple comparisons, p values were corrected using the Bonferroni–Holm method (p_{BH}).

A matrix was built containing the total set of formulae assigned in raw and chlorinated samples and their spectral abundances. Multivariate analyses (Principal Component Analysis, PCA) were carried out in order to elucidate trends among samples and to identify those features that better distinguished chlorinated from raw samples. Correlation among variables and principal components (PC) was quantified as the square cosine of their angle in the loading graph, which may range from 0 ($\alpha = 90°$: orthogonal, totally uncorrelated) to 1 ($\alpha = 0°$: parallel, perfectly correlated).

The dissimilarity among samples was explored using the function vegan:vegdist and represented with hierarchical clustering dendrograms (stats:heatmap).

The statistical dependence between THMs/HANs and the HRMS formulae were assessed in terms of Spearman's rank correlation. Only those formulae that had been detected in 70% of the samples were considered. Those pairs of variables that were correlated with Spearman's rank coefficients $\rho \geq 0.625$ and $\rho \geq 0.795$ were considered to be "statistically correlated" and "strongly correlated", respectively. These thresholds imply correlations with statistical significances of, approximately, $p \leq 5.00 \times 10^{-2}$ and $p \leq 5.00 \times 10^{-3}$, respectively, according to equation (4):

$$t \approx \rho \sqrt{\frac{n-2}{1-\rho^2}}, \quad (4)$$

where n is the number of observations and t is the Student's T statistic, which is justified by the permutation argument (Kendall and Stuart, 1969).

2.8. Additional precautions and safety considerations

In order to avoid sample contamination, all the lab glassware employed in these experiments had been thoroughly cleaned as follows: (i) washed with detergent, (ii) immersed in nitric acid bath (HNO_3 10% v/v) overnight, (iii) rinsed with ultrapure water, (iv) rinsed with acetone and (v) thoroughly dried with nitrogen. Experiments were carried out under extraction fume.

3. Results and discussion

3.1. Data treatment and study of samples by hierarchical clustering analysis

Table 2 summarises the main characteristics of the infused spectra, distinguishing raw samples from chlorinated ones. As can be seen, the infusion of the raw extracts offered spectra with ~85,000 ± 3000 peaks, most of which (approx. 90%) were found to be noise and low-intensity artefacts. Once cleaned up, spectra presented an average number of monoisotopic signals of ~6800 ± 200. This value was relatively constant through the different samples and no significant trends were observed linking the number of signals and the sampling point or the depth of the water column.

Peaks were tentatively assigned to empirical formulae using a custom R script (Text S2). A matrix was built containing the detected features and their respective abundance in each sample. Samples were classified according to their dissimilarity by measuring their "Cao dissimilarity index" (CYd) (Cao et al., 1997). The resulting dendrogram (Fig. S1) satisfactorily grouped samples according to their two main characteristics: matrix (river or reservoir water) and water body (Ter River, Sau, Susqueda and Pasteral). Once the chlorinated samples were introduced into the model (Fig. S2), the type of treatment (raw or chlorinated sample) became the primary factor that drove the clustering. This highlights that water chlorination had a decisive impact in the elemental composition of DOM.

3.2. Effects of chlorination to organic matter spectra and its KMD

As can be seen in Table 2, the number of signals detected by ESI(−) significantly increased after chlorination ($p = 0.0003$), from 8475 ± 297 to 9559 ± 721. Accordingly, the number of peaks corresponding to monocharged molecules/fragments with exclusively ^{12}C atoms increased from 6832 ± 235 to 8418 ± 247 ($p < 10^{-4}$).

In parallel, the average intensity of these peaks decreased significantly (ratio, 0.71; $p = 0.0003$). More precisely, their average m/z, weighted by intensity, decreased from m/z ~361 ± 9 to ~345 ± 15 ($p = 0.0051$). These changes imply the breakage of larger molecules to create smaller, less intense, transformation products, which can be attributed to miscellaneous oxidative degradation reactions of DOM.

KMD plots corroborated a decrease in the average molecular mass of the spectra after chlorination. The number of peaks with $m/z > 600$ was lower after chlorination, as it is exemplified in Fig. 3, which shows the KMD plots of the Pasteral extracts, and the dataset was compressed in a narrower m/z window. This behaviour was observed in the whole set of KMD plots (which are collected in Fig. S3 in the Supporting Information).

In parallel, the average KMD and the intensity-averaged KMD decreased significantly ($p = 0.0051$ and $p = 0.0093$) after chlorination. As a general rule, low KMD values can be related to hydrogen-poorer molecules (e.g. aromatic compounds to the detriment of aliphatic molecules) (Nikolic, 2011) and more oxidized molecules (see Table S2). From a mechanistic point of view, this can be justified by the oxidation of hydroxyls to carbonyls, which produces aldehydes and ketones from primary and secondary alcohols, respectively (Deborde and Von Gunten, 2008; Hu et al., 2003). KMD can also decrease as a result of the hydrolysis of ketones, which produces highly oxidized molecules, such as monohydroxyl acetone, dihydroxyl acetone and, ultimately, lactate. Finally, a decrease in the KMD can be justified because of the introduction of halogens to the molecular structure.

3.3. Determination of elemental composition and effects of chlorination on the VK regions

The DOM profiles of every sample were fingerprinted building VK diagrams based on the O/C and H/C ratios of each identified formulae. Fig. S4, in the Supplementary Information, collects the whole set of VK diagrams, detailing the intensity and m/z of each feature with the size and colour of the scattered points. VK diagrams were used to automatically classify the detected features in VK compositional spaces defined by their O/C and H/C ratios. Fig. 3 shows a VK diagram of Pasteral's surface water (raw and

Table 2
Comparison of data obtained in raw and chlorinated samples. Normally distributed data are highlighted with a dagger (†), and those groups of data that are statistically different ($p < 0.0500$) are highlighted with an asterisk (*).

	Raw samples (average ± st.dev)	Chlorinated (average ± st.dev)	Ratio of averages	Comparison
No. of peaks (including noise)	85,530 ± 3013	88,430 ± 1675	1.04	p = 0.0124 *
Noise threshold (a.u.)	65 ± 12†	59 ± 11†	0.90	p = 0.1931
Number of signals (S/N > 3)	8475 ± 297†	9559 ± 721†	1.13	p = 0.0003 *
Intensity (a.u.)	6017 ± 1,188†	4288 ± 837†	0.71	p = 0.0003 *
m/z	394.2714 ± 14.3346	357.9249 ± 8.4016†	0.91	p = 0.0051 *
Intensity-weighted m/z	360.9601 ± 9.2478	344.5953 ± 14.8454	0.95	p = 0.0051 *
KMD	0.3263 ± 0.0155	0.2983 ± 0.0110†	0.91	p = 0.0051 *
Intensity-weighted KMD	0.2983 ± 0.0110	0.2773 ± 0.0078	0.97	p = 0.0093 *
O/C	0.4264 ± 0.0139†	0.4290 ± 0.0120	1.01	p = 0.5093
Intensity-weighted O/C	0.4291 ± 0.0182†	0.4321 ± 0.0172	1.01	p = 0.5093
H/C	1.0589 ± 0.0248†	1.0480 ± 0.0254	0.99	p = 0.2846
Intensity-weighted H/C	1.1774 ± 0.0197†	1.1703 ± 0.0121	0.99	p = 0.2846
N/C	0.0438 ± 0.0058	0.0457 ± 0.0079	1.04	p = 0.3576
Intensity-weighted N/C	0.0080 ± 0.0070	0.0089 ± 0.0084	1.12	p = 0.1676

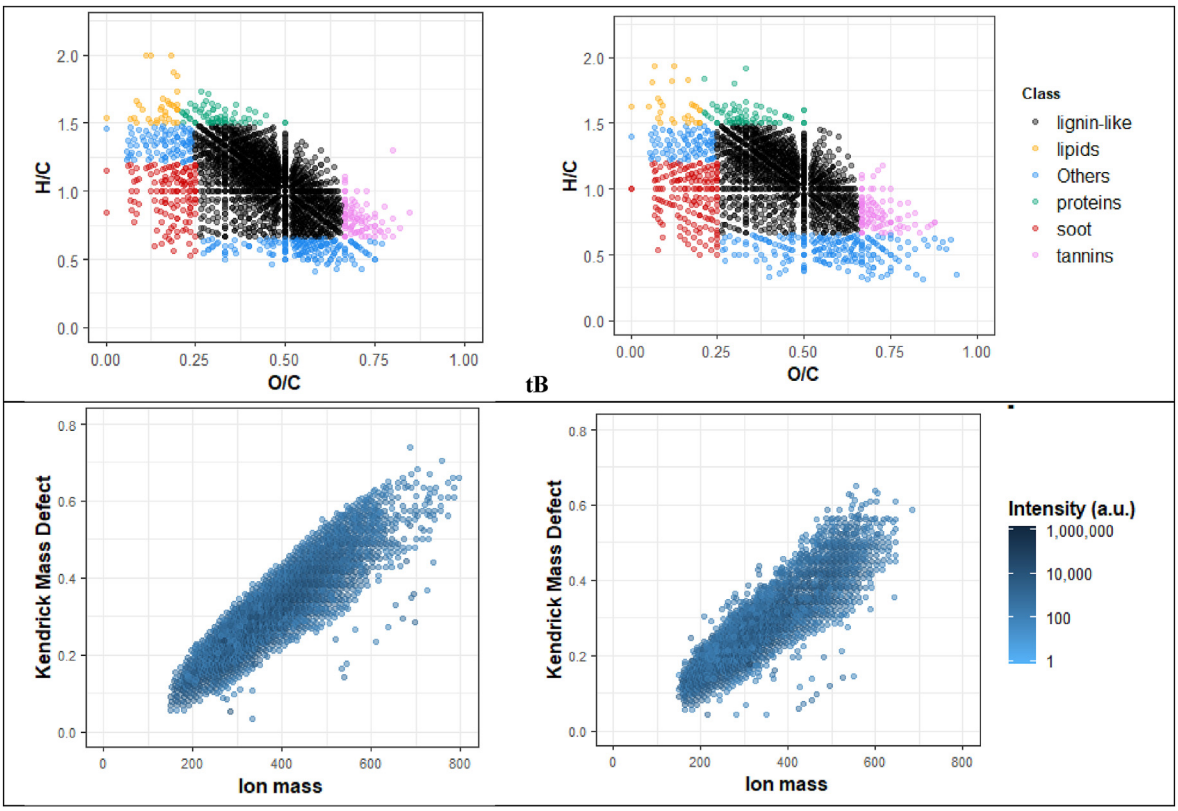

Fig. 3. VK diagrams (above) and KMD plots (above) of Pasteral reservoir, analysed before (left) and after (right) chlorination.

Table 3
Behaviour of features during chlorination according to their compositional space in the VK diagrams. Those values highlighted in bold font belong to the predominant trend in their corresponding VK region.

Subset of m/z		Number of signals that …					
	Main VK regions	… disappeared	… decreased	… didn't change	… increased	… appeared	Total
Full dataset	Lignin-like	1225 (34.7%)	1005 (28.5%)	606 (17.2%)	91 (2.58%)	605 (17.1%)	3532
	Tannin-like	59 (18.1%)	11 (3.37%)	108 (33.1%)	18 (5.52%)	130 (39.9%)	326
	Condensed hydrocarbon-like	203 (33.7%)	15 (2.49%)	188 (31.2%)	54 (8.96%)	143 (23.7%)	603
	Lipids-like	69 (56.6%)	13 (10.7%)	18 (14.8%)	0 (0%)	22 (18.0%)	122
	Protein-like	55 (23.7%)	40 (17.2%)	50 (21.6%)	12 (5.17%)	75 (32.3%)	232
Subset of halogenated signals	Lignin-like	129 (21.29%)	0 (0%)	16 (2.64%)	1 (0.17%)	460 (75.91%)	606
	Tannin-like	0 (0%)	0 (0%)	0 (0%)	0 (0%)	31 (100%)	31
	Condensed hydrocarbon-like	138 (49.11%)	1 (0.36%)	37 (13.17%)	2 (0.71%)	103 (36.65%)	281
	Lipids-like	43 (63.24%)	0 (0%)	8 (11.76%)	0 (0%)	17 (25%)	68
	Protein-like	27 (36%)	0 (0%)	2 (2.67%)	0 (0%)	46 (61.33%)	75

chlorinated extracts, on the left and right respectively), with their compositional spaces clearly delimited.

Table 3 summarises the relative abundances and behaviour of the features according to their location in the VK diagram. The group of features placed in the "lignin-like features" region was the most abundant in the analysed samples: 3532 peaks belonged to this compositional space, equivalent to ~73% of the total number of signals, which can be expected in common natural surface waters with no significant anthropogenic pressure. In freshwater DOM's VK diagram, this compositional space is shared by lignin-related molecules (and ESI fragments), and signals related to carboxyl-rich alicyclic molecules (CRAM) (Lam et al., 2007), among other organic substances with the same compositional characteristics.

The number of features assigned to this region decreased both, in absolute and in relative terms, after chlorination. 1005 signals corresponding to lignin-like signals decreased their intensity according to Wilcoxon signed-rank tests or paired Student's *t* tests ($p < 0.05$) and 1225 signals disappeared completely. The abundances of 606 lignin-like features were unaltered. Only 91 features increased their concentrations and, finally, 665 new lignin-like peaks appeared after chlorination. Among the latter, 460 were assigned to halogenated formulae.

While the lignin-like region decreased in terms of intensity and number of peaks, it is no less true that it accumulated the highest number of new signals, highlighting the complex behaviour of the lignin fraction during water chlorination. Lignin is composed of complex mixtures of polymers based on phenol moieties (guaiacyl, syringyl, and *p*-hydroxyphenylpropane aromatic moieties) (National Research Council (US) Safe Drinking Water Committee, 1979), the chlorination of which is an importance source of halogenated DBPs (Chuang et al., 2015).

Lyon et al. (2014) also observed that fluorescent organic matter

corresponding to the Parallel Factor Analysis (PARAFAC) component C3 showed the highest reactivity to chlorination. This component is associated with terrestrial humic-like features, which include lignin breakdown products, degraded lignin and other aromatic intricate molecules. In the present work, the number of peaks tentatively related to soil-derived humics (defined in Šantl-Temkiv et al. (2013) as H/C < 1.5 and A.I. ≤ 0.5) also decreased from 2088 ± 133 to 1768 ± 157 ($p = 0.0001$) and their average intensity decreased by 65%.

On another note, the number of peaks assigned as "lipids-like features" and "condensed hydrocarbon-like features" also decreased: Most lipids-like signals that had been detected in the original samples (56.6%) disappeared after chlorination and 11.0% significantly decreased their abundance ($p < 0.05$). Similarly, 203 condensed hydrocarbon-like features disappeared during the treatment. A total number of 143 new features appeared in the condensed hydrocarbon-like compositional compartment (103 of which, halogenated) and 22 new signals (17 of which halogenated) appeared in the lipid-like compartment after chlorination.

Chlorination caused the appearance of several new highly-oxidized molecules, with O/C ratios >0.75 (see, for example, the VK diagram in Fig. 3), a significant part of which belonged to the "tannin-like" region. The average O/C ratio of those new formulae was 0.767 ± 0.080, significantly higher ($p < 10^{-4}$) than the O/C ratio of the other registered tannin-like *m/z* (0.717 ± 0.054). In parallel, the appearance of features with low H/C ratios (H/C < 0.5) was also observed.

In the present work, up to 1061 halogenated formulae were determined (Table 3). Naturally occurring halogenated features were mainly detected in the condensed hydrocarbon-like and the lignin-like regions (178 and 146 features, respectively). The number of halogenated features increased, as expected, after chlorination, particularly in the lignin-like region (460 new halogenated features). Up to 657 new halogenated features were identified. These halogenated signals are highlighted in the individual VK diagrams of each sample (Fig. S5 and Fig. S6 for chlorinated and brominated features, respectively). As it can be seen, most of the halogenated features occurring in natural water samples presented an O/C ratio lower than 0.5, while a large fraction of the new formulae was significantly more oxidized (O/C > 0.5).

The analytical method that was employed in the present work, involving SPE under vacuum and ESI-HRMS analysis, is not able to efficiently capture and detect commonly targeted DBPs because of their physicochemical properties (i.e., their typically high vapour pressures and low molecular masses). Therefore, those peaks assigned as halogenated features in the present study likely were related to semivolatile/non-volatile components/fragments of halogenated DOM, which can occur by progressive halogenations of the α-carbon of carbonyl groups (for example, the haloform reaction (Morris, 1975)), the addition of halogens to double bonds (Ghanbari et al., 1983) and the additions to phenol rings (Gallard and von Gunten, 2002).

3.4. Classification of samples by PCA

In order to better understand the factors that differentiated raw and chlorinated samples, a PCA model was performed. The first two principal components, PC1 and PC2, explained 70.9% of the data variance (see the main PCs' eigenvalues in Fig. S7). The separation of chlorinated and untreated samples was clear in the score graphs of PC1 *vs*. PC2 (Fig. 4): chlorinated samples were related to low values of PC1 while untreated samples were related to high values of PC1.

PC1 was, therefore, closely related to samples chlorination. This PC was correlated with the concentrations of certain substances with the general formula $C_xH_yO_z$. Table S3 lists those formulae the abundances of which were more closely correlated to PC1. As can be observed, their H/C ratios were compressed between 0.75 and 1.14 and their O/C ratios ranged from 0.37 to 0.52. This is in agreement with Zhang et al. (2012), where it was observed that "compounds with low degree of oxidation are more reactive toward free chlorine" in surface water from Shanghai and Beijing catchment areas. These features, located in the lignin-like region of the VK-diagram, presented negligible nitrogen content, a DBE/C that ranged from 0.50 to 0.69 and an A.I. ≤ 0.38. Their DBE/C ratio suggests the prevalence of aromatic structures (0.66 > DBE/C > 0.5) and, according to their H/C ratio and A.I., they can be tentatively related to "soil-derived humics" (H/C < 1.5 and A.I. ≤ 0.5), as discussed by Šantl-Temkiv et al. (2013). However, further instrumental analyses should be carried out to unambiguously identify their structure.

These tentatively identified humic-derived lignin-like features were highly intercorrelated (see Fig. S8) and sample chlorination decreased their intensity in a statistically significant manner (p_{BH} values from 0.0009 to 0.0020). The Ter sample exhibited a particularly low abundance of these lignin-like features, with concentrations of the same order than chlorinated samples, which probably justified its clustering in the dendrogram (Fig. S2).

3.5. Disinfection by-products formation potentials and correlation with HRMS features

The THMs and HANs FPs are detailed in Table 1. THMs FP ranged from 33.6 to 75.9 μg/L (54 ± 14 μg/L) and HANs FP ranged between 1.4 and 5.1 μg/L (3.8 ± 1.2 μg/L). The concentrations of THMs were, as expected, significantly higher than those of HANs and followed a relatively close trend: THMS FP and HANs FP correlated with a Pearson correlation coefficient of $r = 0.59$ and a Spearman's rank correlation coefficient of $\rho = 0.74$.

TOC was a satisfactory predictor of THMs FP ($R^2 = 0.60$ and $\rho = 0.77$) but it was a poor predictor of HANs FP ($R^2 = 0.24$ and $\rho = 0.37$). Similarly, total nitrogen (TN) inversely correlated with THMs FP ($R^2 = 0.58$ and $\rho = -0.63$) but was inadequately correlated with HANs FP ($R^2 = 0.14$ and $\rho = -0.09$). These results highlight the need to find more specific descriptors to understand the behaviour of a wider range of halogenated DBPs.

THMs FP and HANs FP were compared to the intensities of those features that had been detected in, at least, 7 of the 10 analysed samples. A total of 516 peaks were found to be correlated to THMs FP ($\rho \geq 0.625$) and 208 of them were "strongly correlated" ($\rho \geq 0.795$). Fig. 5 shows the VK diagram with signals being represented as a function of ρ: As can be seen, the strongly correlated signals were mostly lignin-like and/or CRAM features (H/C ranging from 0.71 to 1.6 and O/C ratios ranging from 0.06 to 0.52. These features also presented a very low nitrogen content (average N/C = 0.005). Interestingly, the formulae in Fig. 5, strongly correlated to THMs FP, are similar to those peaks (listed in Table S3) that, in the multivariate analyses, were good descriptors of chlorinated/raw samples differentiation. However, while both sets of peaks are similar in composition ($C_xH_yO_z$), in H/C ratio and in O/C ratio, only four particular features ($C_{13}H_{18}O_3$, $C_{15}H_{14}O_5$, $C_{15}H_{16}O_5$ and $C_{15}H_{20}O_3$) were members of both lists, corroborating that the formation of THMs is just one of the multiple reactions that affect DOM during water chlorination.

Similar to our results, Hua et al. (2015) also observed that the formation of THMs and trihaloacetic acids during water chlorination was correlated with $SUVA_{254}$, which is related to the presence of UV-absorbing molecules containing labile double bonds and aromatic rings. Also Beauchamp et al. (2018) found that differential UV absorbance and THMs concentrations were correlated with $0.62 \leq R^2 \leq 0.99$. Our results suggest that these compounds were

Fig. 4. Score plot of PCA with scaled data, representing samples in PC1 and PC2 axis. Chlorinated samples are presented in red while untreated samples are displayed in blue. The two ellipses were generated automatically highlighting an area with a 95% of possibility to containing samples of their kind. (For interpretation of the references to colour in this figure legend, the reader is referred to the Web version of this article.)

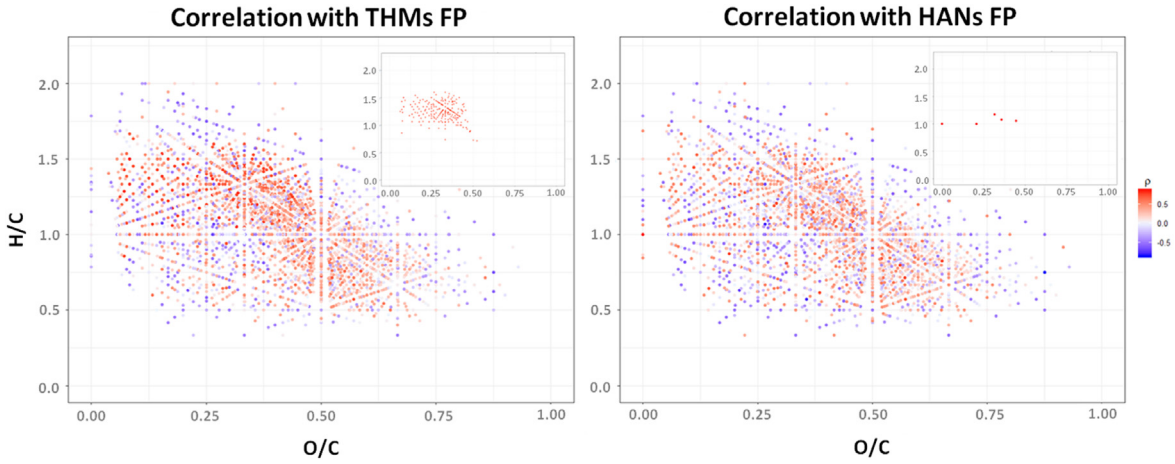

Fig. 5. VK diagram showing the Spearman correlation of THMs (left) and HANs (right) the formulae that were found in 70% of the samples. The miniature diagrams located the up-right corners content only those features that were strongly ($\rho \geq 0.795$) correlated to THMs and HANs FP, respectively.

particularly located in the lignin-like compositional space of the van Krevelen's DOM.

On another note, the number of features that correlated with HANs FP was smaller: 60 features were correlated with statistical significance ($\rho \geq 0.625$) and only 5 could be labelled as "strongly correlated" ($\rho \geq 0.795$). These features are good candidates to be used as predictors of HANs FP. These peaks were plotted in the lignin-like region, in a relatively narrow H/C *vs* O/C window (H/C ranging from 1.0 to 1.2 and O/C ranging from 0.19 to 0.49). Their nitrogen content was significantly high (average N/C = 0.49), which is expected considering that HANs are *N*-containing DBPs. The ternary VK diagrams illustrate the differences in the N/C ratios of those features related to THMs FP (Fig. S9) and those related to HANs FP (Fig. S10).

4. Conclusions

The primary object of this study was to better understand how water chlorination modified the DOM fingerprint obtained with HRMS. Our results obtained from 10 different surface water samples showed that water chlorination indeed produced significant changes in the composition of DOM and, subsequently, in their HRMS spectra. Chlorinated samples exhibited signals with smaller m/z, lower KMD and, as expected, a higher number of halogenated features. These changes were studied at fingerprinting level and from a multivariate analyses perspective.

Significant changes were observed in the regions of the lignin-like/CRAM, the soil humics, and that of the fatty acids-like features, where several signals disappeared during chlorination, as

well as in the condensed hydrocarbon region, where several new features, halogenated and non-halogenated, were detected. In the tannin-like region, several new features, primarily corresponding to highly oxidized formulae, were also detected. Overall, these changes sufficed to successfully classifying the analysed samples according to their treatment status (raw/chlorinated) and origin, via hierarchical clustering analyses and PCA scores.

In PCA it was concluded that sample chlorination (related to PC1) primarily involved a decrease in the concentration of non-nitrogenized lignin-like features. Up to 28 signals were found to be highly correlated ($\cos^2(\alpha) > 0.95$) to sample chlorination, all of them with $C_xH_yO_z$ formulae and elemental ratios (H/C & O/C) characteristic from the ligning-like/CRAM compositional space.

Finally, we identified two regions of the VK diagram, located within the lignin-like features, that were strongly correlated ($\rho \geq 0.795$) to THMs and HANs FP. To the best of our knowledge, the present work is the first to identify surrogates of HAN generation during chlorination of surface waters.

Recently, Williams et al. (2019) described how removing certain portions of the DOM pool, in real plant scale, significantly decrease the formation potential of individual chlorinated and brominated DBPs. Our study is a promising step towards identifying appropriate surrogates capable of anticipating the risk that chlorination DBPs may pose for the final consumer, offering a higher selectivity than unspecific techniques, such as TOC and $SUVA_{254}$ measurements. Moreover, this approach may be applied to other relevant families of DBPs. However, with the current results, it is not possible to unambiguously affirm that these features correspond to direct precursors of THMs and HANs. Further studies should be conducted (e.g. using liquid chromatography coupled to HRMS, curated libraries and standards) to univocally identify compounds and individually test their DBPs FP. However, our results clearly indicate that these two regions of the VK diagram play a crucial role in the formation of the analysed DBPs.

Declaration of competing interest

The authors declare that they have no known competing financial interests or personal relationships that could have appeared to influence the work reported in this paper.

Acknowledgements

This project was funded by the Spanish Ministry of Science, Innovation and Universities, AEI-MICIU, and the European Fund for Regional Development under the National Program for Research Aimed at the Challenges of Society, through the project NDMA_P-redict (CTM 2017-85335-R); and by the European Union's Horizon 2020 Research and Innovation Programme, through the MANTEL-ITN Project (Grant No: 722518). The authors thank Generalitat de Catalunya through Consolidated Research Group ENV 2017 SGR 1124 and Tech 2017 SGR 1318. ICRA researchers thank funding from CERCA program. MJF acknowledges her Ramón y Cajal fellowship (RyC-2015-17108), from the AEI-MICIU; AJG acknowledges his PhD scholarship from AGAUR (2019FI_B2_00202), from the Government of Catalonia; PGF acknowledges SmartWorkflow, which has received funding from the European Union's Horizon 2020 R&I program under grant 791235. The authors would like to thank the staff of the Scientific and Technical Services of the Catalan Institute of Water Research for their invaluable assistance.

Appendix A. Supplementary data

Supplementary data to this article can be found online at https://doi.org/10.1016/j.watres.2020.115743.

References

Agència Catalana de l'Aigua, 2019. Agència Catalana de l'Aigua Website: Generalitat de Catalunya [WWW Document]. http://aca.gencat.cat/ca/laigua/consulta-de-dades/geoserveis/. accessed 10.15.19.
Agència Catalana de l'Aigua, 2015. Pla de gestió del districte de conca fluvial de Catalunya 2016-2021.
Andersson, A., Harir, M., Gonsior, M., Hertkorn, N., Schmitt-Kopplin, P., Kylin, H., Karlsson, S., Ashiq, M.J., Lavonen, E., Nilsson, K., 2019. Waterworks-specific composition of drinking water disinfection by-products. Environ. Sci. Water Res. Technol. 5, 861–872.
APHA, PHA, 2005. AWWA and WPCF Standard Methods for the Examination of Waters and Waste Waters.
Arakawa, N., Aluwihare, L.I., Simpson, A.J., Soong, R., Stephens, B.M., Lane-Coplen, D., 2017. Carotenoids are the likely precursor of a significant fraction of marine dissolved organic matter. Sci. Adv. 3, e1602976.
Beauchamp, N., Laflamme, O., Simard, S., Dorea, C., Pelletier, G., Bouchard, C., Rodriguez, M., 2018. Relationships between DBP concentrations and differential UV absorbance in full-scale conditions. Water Res. 131, 110–121.
Cao, Y., Williams, W.P., Bark, A.W., 1997. Similarity measure bias in river benthic Aufwuchs community analysis. Water Environ. Res. 69, 95–106.
Chinese Department of Health, 2006. GB5749-2006. P.R. China Standards for Drinking Water Quality.
Chu, W.-H., Gao, N.-Y., Deng, Y., Krasner, S.W., 2010. Precursors of dichloroacetamide, an emerging nitrogenous DBP formed during chlorination or chloramination. Environ. Sci. Technol. 44, 3908–3912.
Chuang, Y.-H., McCurry, D.L., Tung, H., Mitch, W.A., 2015. Formation pathways and trade-offs between haloacetamides and haloacetaldehydes during combined chlorination and chloramination of lignin phenols and natural waters. Environ. Sci. Technol. 49, 14432–14440.
Commission, E., 1998. Council Directive 98/83/EC of 3 November 1998 on the quality of water intended for human consumption. Off. J. Eur. communities 41, 32–54.
De Vera, G.A., Stalter, D., Gernjak, W., Weinberg, H.S., Keller, J., Farré, M.J., 2015. Towards reducing DBP formation potential of drinking water by favouring direct ozone over hydroxyl radical reactions during ozonation. Water Res. 87, 49–58.
Deborde, M., Von Gunten, U.R.S., 2008. Reactions of chlorine with inorganic and organic compounds during water treatment—kinetics and mechanisms: a critical review. Water Res. 42, 13–51.
Dittmar, T., Koch, B.P., 2006. Thermogenic organic matter dissolved in the abyssal ocean. Mar. Chem. 102, 208–217.
Doederer, K., Gernjak, W., Weinberg, H.S., Farré, M.J., 2014. Factors affecting the formation of disinfection by-products during chlorination and chloramination of secondary effluent for the production of high quality recycled water. Water Res. 48, 218–228.
EPA., U.S., 2000. The History of Drinking Water Treatment.
European Parliament, 2000. Directive 2000/60/EC of the European Parliament and of the Council of 23 October 2000 establishing a framework for Community action in the field of water policy. Off. J. Eur. Parliam. L327, 1–82.
Farré, M.J., Jaén-Gil, A., Hawkes, J., Petrovic, M., Catalán, N., 2019. Orbitrap molecular fingerprint of dissolved organic matter in natural waters and its relationship with NDMA formation potential. Sci. Total Environ. 670, 1019–1027.
Font-Ribera, L., Gràcia-Lavedan, E., Aragonés, N., Pérez-Gómez, B., Pollán, M., Amiano, P., Jiménez-Zabala, A., Castaño-Vinyals, G., Roca-Barceló, A., Ardanaz, E., 2018. Long-term exposure to trihalomethanes in drinking water and breast cancer in the Spanish multicase-control study on cancer (MCC-Spain). Environ. Int. 112, 227–234.
Gallard, H., von Gunten, U., 2002. Chlorination of phenols: kinetics and formation of chloroform. Environ. Sci. Technol. 36, 884–890.
Ghanbari, H.A., Wheeler, W.B., Kirk, J.R., 1983. Reactions of chlorine and chlorine dioxide with free fatty acids, fatty acid esters, and triglycerides. Water chlorination Environ. impact Heal. Eff. 4.
Hawkes, J.A., Dittmar, T., Patriarca, C., Tranvik, L., Bergquist, J., 2016. Evaluation of the Orbitrap mass spectrometer for the molecular fingerprinting analysis of natural dissolved organic matter. Anal. Chem. 88, 7698–7704.
Hawkes, J.A., Radoman, N., Bergquist, J., Wallin, M.B., Tranvik, L.J., Löfgren, S., 2018. Regional diversity of complex dissolved organic matter across forested hemiboreal headwater streams. Sci. Rep. 8, 16060.
Hou, M., Chu, W., Wang, F., Deng, Y., Gao, N., Zhang, D., 2018. The contribution of atmospheric particulate matter to the formation of CX3R-type disinfection by-products in rainwater during chlorination. Water Res. 145, 531–540.
Hu, J., Cheng, S., Aizawa, T., Terao, Y., Kunikane, S., 2003. Products of aqueous chlorination of 17β-estradiol and their estrogenic activities. Environ. Sci. Technol. 37, 5665–5670.
Hua, G., Reckhow, D.A., 2007. Comparison of disinfection byproduct formation from chlorine and alternative disinfectants. Water Res. 41, 1667–1678.
Hua, G., Reckhow, D.A., Abusallout, I., 2015. Correlation between SUVA and DBP formation during chlorination and chloramination of NOM fractions from different sources. Chemosphere 130, 82–89.
Hughey, C.A., Hendrickson, C.L., Rodgers, R.P., Marshall, A.G., Qian, K., 2001. Kendrick mass defect spectrum: a compact visual analysis for ultrahigh-resolution broadband mass spectra. Anal. Chem. 73, 4676–4681.
Kellerman, A.M., Dittmar, T., Kothawala, D.N., Tranvik, L.J., 2014. Chemodiversity of

dissolved organic matter in lakes driven by climate and hydrology. Nat. Commun. 5, 3804.
Kendall, M.G., Stuart, A., 1969. Inference and Relationship (Hafner).
Kendrick, E., 1963. A mass scale based on CH2= 14.0000 for high resolution mass spectrometry of organic compounds. Anal. Chem. 35, 2146–2154.
Kim, S., Kramer, R.W., Hatcher, P.G., 2003. Graphical method for analysis of ultrahigh-resolution broadband mass spectra of natural organic matter, the van Krevelen diagram. Anal. Chem. 75, 5336–5344.
Koch, B.P., Dittmar, T., 2006. From mass to structure: an aromaticity index for high-resolution mass data of natural organic matter. Rapid Commun. Mass Spectrom. 20, 926–932.
Lam, B., Baer, A., Alaee, M., Lefebvre, B., Moser, A., Williams, A., Simpson, A.J., 2007. Major structural components in freshwater dissolved organic matter. Environ. Sci. Technol. 41 (24), 8240–8247. https://doi.org/10.1021/es0713072.
Lavonen, E.E., Gonsior, M., Tranvik, L.J., Schmitt-Kopplin, P., Kǫhler, S.J., 2013. Selective chlorination of natural organic matter: identification of previously unknown disinfection byproducts. Environ. Sci. Technol. 47, 2264–2271.
Lê, S., Josse, J., Husson, F., 2008. FactoMineR: an R package for multivariate analysis. J. Stat. Software 25, 1–18.
Leal, J.L., Fuller, G.W., Johnson, G.A., 1909. The Sterilization Plant of the Jersey City Water Supply Company at Boonton. Amer. Water Works Assoc, NJ.
Lee, J., Ha, K.-T., Zoh, K.-D., 2009. Characteristics of trihalomethane (THM) production and associated health risk assessment in swimming pool waters treated with different disinfection methods. Sci. Total Environ. 407, 1990–1997.
Li, Y., Harir, M., Lucio, M., Kanawati, B., Smirnov, K., Flerus, R., Koch, B.P., Schmitt-Kopplin, P., Hertkorn, N., 2016. Proposed guidelines for solid phase extraction of Suwannee River dissolved organic matter. Anal. Chem. 88, 6680–6688.
Li, Y., Harir, M., Uhl, J., Kanawati, B., Lucio, M., Smirnov, K.S., Koch, B.P., Schmitt-Kopplin, P., Hertkorn, N., 2017. How representative are dissolved organic matter (DOM) extracts? A comprehensive study of sorbent selectivity for DOM isolation. Water Res. 116, 316–323.
Liu, P., Farré, M.J., Keller, J., Gernjak, W., 2016. Reducing natural organic matter and disinfection by-product precursors by alternating oxic and anoxic conditions during engineered short residence time riverbank filtration: a laboratory-scale column study. Sci. Total Environ. 565, 616–625.
Lyon, Bonnie A., Corey, Rose M., Weinberg, Howard S., 2014. Changes in dissolved organic matter fluorescence and disinfection byproduct formation from UV and subsequent chlorination/chloramination. J. Hazard Mater. 264, 411–419. https://doi.org/10.1016/j.jhazmat.2013.10.065.
Melendez-Perez, J.J., Martínez-Mejia, M.J., Eberlin, M.N., 2016. A reformulated aromaticity index equation under consideration for non-aromatic and non-condensed aromatic cyclic carbonyl compounds. Org. Geochem. 95, 29–33.
Morris, J.C., 1975. Formation of Halogenated Organics by Chlorination of Water Supplies: a Review. Office of Research and Development, US Environmental Protection Agency.
National Research Council (US) Safe Drinking Water Committee, 1979. The Chemistry of Disinfectants in Water: Reactions and Products. Environmental Protection Agency, Office of Drinking Water.
NHMRC, NRMMC, 2011. Australian Drinking Water Guidelines Paper 6 National Water Quality Management Strategy. National Health and Medical Research Council, National Resource Management Ministerial Council, Commonwealth of Australia, Canberra. ISBN: 1864965118. Downloaded from. https://www.nhmrc.gov.au/about-us/publications/australian-drinking-water-guidelines#block-views-block-file-attachments-content-block-1.
Nikolic, G., 2011. Fourier Transforms: Approach to Scientific Principles. BoD–Books on Demand.
Oksanen, J., Blanchet, F.G., Friendly, M., Kindt, R., Legendre, P., McGlinn, D., Minchin, P.R., O'Hara, R.B., Simpson, G.L., Solymos, P., Stevens, M.H.H., Szoecs, E., Wagner, H., 2019. Vegan: Community Ecology Package. R Package Version 1.17-4. vegan Community Ecol. Packag. R Packag version 2.5-4. https://CRAN.R-project.org/package=vegan.
Patriarca, C., Bergquist, J., Sjǿberg, P.J.R., Tranvik, L., Hawkes, J.A., 2018. Online HPLC-ESI-HRMS method for the analysis and comparison of different dissolved organic matter samples. Environ. Sci. Technol. 52, 2091–2099.
Peng, D., Saravia, F., Abbt-Braun, G., Horn, H., 2016. Occurrence and simulation of trihalomethanes in swimming pool water: a simple prediction method based on DOC and mass balance. Water Res. 88, 634–642.
R Core Team, 2019. A Language and Environment for Statistical Computing. R Foundation for Statistical Computing, Vienna, Austria, 2012. https://www.R-project.org.
Richardson, S.D., Ternes, T.A., 2018. Water analysis: emerging contaminants and current issues. Anal. Chem. 90, 398–428.
Richardson, S.D., Thruston Jr., A.D., Krasner, S.W., Weinberg, H.S., Miltner, R.J., Schenck, K.M., Narotsky, M.G., McKague, A.B., Simmons, J.E., 2008. Integrated disinfection by-products mixtures research: comprehensive characterization of water concentrates prepared from chlorinated and ozonated/postchlorinated drinking water. J. Toxicol. Environ. Health Part A 71, 1165–1186.
Riedel, T., Zark, M., Vähätalo, A.V., Niggemann, J., Spencer, R.G.M., Hernes, P.J., Dittmar, T., 2016. Molecular signatures of biogeochemical transformations in dissolved organic matter from ten world rivers. Front. Earth Sci. 4, 85.
Roccaro, P., Vagliasindi, F.G.A., Korshin, G.V., 2009. Changes in NOM fluorescence caused by chlorination and their associations with disinfection by-products formation. Environ. Sci. Technol. 43, 724–729.
Šantl, Temkiv, T., Finster, K., Dittmar, T., Hansen, B.M., Thyrhaug, R., Nielsen, N.W., Karlson, U.G., 2013. Hailstones: a window into the microbial and chemical inventory of a storm cloud. PloS One 8, e53550.
Schum, S., Mazzoleni, L., Brown, L., 2019. MFAssignR: Molecular Formula Assignment Using CHOFIT Algorithm. R package version 0.0.5.
Schymanski, E.L., Jeon, J., Gulde, R., Fenner, K., Ruff, M., Singer, H.P., Hollender, J., 2014. Identifying Small Molecules via High Resolution Mass Spectrometry: Communicating Confidence.
Sohn, J., Amy, G., Cho, J., Lee, Y., Yoon, Y., 2004. Disinfectant decay and disinfection by-products formation model development: chlorination and ozonation by-products. Water Res. 38, 2461–2478.
Traube, M., 1894. Einfaches Verfahren Wasser in grossen Mengen keimfrei zu machen. Med. Microbiol. Immunol. 16, 149–150.
US-EPA, 2006. Stage 2 Disinfectants and Disinfection Byproducts Rule (Stage 2 DBPR) 71 FR 388.
US-EPA, 1998. Stage 1 Disinfectants and Disinfection Byproducts Rule (Stage 1 DBPR) 63 FR 69390.
Villanueva, C.M., Cordier, S., Font-Ribera, L., Salas, L.A., Levallois, P., 2015. Overview of disinfection by-products and associated health effects. Curr. Environ. Heal. reports 2, 107–115.
Williams, C.J., Conrad, D., Kothawala, D.N., Baulch, H.M., 2019. Selective removal of dissolved organic matter affects the production and speciation of disinfection byproducts. Sci. Total Environ. 652, 75–84.
Woods, G.C., Simpson, M.J., Kelleher, B.P., McCaul, M., Kingery, W.L., Simpson, A.J., 2009. Online high-performance size exclusion chromatography– nuclear magnetic resonance for the characterization of dissolved organic matter. Environ. Sci. Technol. 44, 624–630.
Yeh, R.Y.L., Farré, M.J., Stalter, D., Tang, J.Y.M., Molendijk, J., Escher, B.I., 2014. Bioanalytical and chemical evaluation of disinfection by-products in swimming pool water. Water Res. 59, 172–184.
Yuthawong, V., Kasuga, I., Kurisu, F., Furumai, H., 2019. Molecular-level changes in dissolved organic matter compositions in lake inba water during KMnO4 oxidation: assessment by Orbitrap mass spectrometry. J. Water Environ. Technol. 17, 27–39.
Zhang, H., Yang, M., 2018. Characterization of brominated disinfection byproducts formed during chloramination of fulvic acid in the presence of bromide. Sci. Total Environ. 627, 118–124.
Zhang, H., Zhang, Y., Shi, Q., Hu, J., Chu, M., Yu, J., Yang, M., 2012. Study on transformation of natural organic matter in source water during chlorination and its chlorinated products using ultrahigh resolution mass spectrometry. Environ. Sci. Technol. 46, 4396–4402. https://doi.org/10.1021/es203587q.
Zhang, H., Zhang, Y., Shi, Q., Zheng, H., Yang, M., 2014. Characterization of unknown brominated disinfection byproducts during chlorination using ultrahigh resolution mass spectrometry. Environ. Sci. Technol. 48, 3112–3119.